# Model-order reduction of electromagnetic fields in open domains

Zimmerling, Jörn; Druskin, Vladimir; Zaslavsky, Mikhail; Remis, Rob F.

**DOI**
10.1190/geo2017-0507.1

**Publication date**
2018

**Document Version**
Final published version

**Published in**
Geophysics

GEOPHYSICS, VOL. 83, NO. 2 (MARCH-APRIL 2018); P. WB61–WB70, 9 FIGS., 2 TABLES.
10.1190/GEO2017-0507.1





# Model-order reduction of electromagnetic fields in open domains

Jörn Zimmerling[1], Vladimir Druskin[2], Mikhail Zaslavsky[2], and Rob F. Remis[1]

## ABSTRACT

We have developed several Krylov projection-based model-order reduction techniques to simulate electromagnetic wave propagation and diffusion in unbounded domains. Such techniques can be used to efficiently approximate transfer function field responses between a given set of sources and receivers and allow for fast and memory-efficient computation of Jacobians, thereby lowering the computational burden associated with inverse scattering problems. We found how general wavefield principles such as reciprocity, passivity, and the Schwarz reflection principle translate from the analytical to the numerical domain and developed polynomial, extended, and rational Krylov model-order reduction techniques that preserve these structures. Furthermore, we found that the symmetry of the Maxwell equations allows for projection onto polynomial and extended Krylov subspaces without saving a complete basis. In particular, short-term recurrence relations can be used to construct reduced-order models that are as memory efficient as time-stepping algorithms. In addition, we evaluated the differences between Krylov reduced-order methods for the full wave and diffusive Maxwell equations and we developed numerical examples to highlight the advantages and disadvantages of the discussed methods.

## INTRODUCTION

Krylov-based electromagnetic (EM) solvers for the Maxwell system in the diffusion approximation have long been the workhorse of the geophysics community (Druskin and Knizhnerman, 1994; Knizhnerman et al., 2009; Börner et al., 2015). In such a solver, the discretized system of equations is projected onto a Krylov subspace in an iterative fashion. The projected system forms a reduced-order model (ROM), from which approximate solutions to the full-order system can be drawn.

ROMs that model electromagnetic wave propagation play an important role in many areas of science and engineering. The application range spans from design optimization of an optical resonator (Zimmerling et al., 2016) and diffusive optical tomography (Kilmer and de Sturler, 2006) to controlled-source EM inversion in the oil and gas industry (Druskin and Zaslavsky, 2007; Borcea et al., 2014). The goal of ROM is usually a reduction in computational load (Antoulas, 2005). In this respect, one can differentiate between two types of applications, namely, applications that require fast construction of an ROM (Druskin and Zaslavsky, 2007) and applications in which an ROM can be constructed offline and is only required to offer accurate and fast evaluation (Budko and Remis, 2004). In many inversion algorithms in geophysics, for example, ROMs that are first computed offline can be used to efficiently evaluate the elements of the Jacobian during the online inversion stage (Borcea et al., 2014). Generally speaking, the online stage of an inversion algorithm is the stage in which one tries to minimize the mismatch between measured data and the data obtained from a simulated configuration. Parametric ROMs can be computed offline and independently of this online inversion stage in case the range of the parameters encountered during inversion is small and known beforehand (Benner et al., 2015). Otherwise, ROMs can be constructed online during each iteration of the inversion algorithm.

In this contribution, we discuss three types of projection-based Krylov model-order reduction techniques for electromagnetic field problems as encountered in geophysics. Polynomial, extended, and rational Krylov subspace (RKS) techniques are presented, and we demonstrate how the structure of the Maxwell equations can be used to efficiently construct ROMs, while preserving the model structure. In particular, we show that the symmetry of the Maxwell's equations allows us to efficiently construct polynomial and extended Krylov bases using short recurrence relations leading to the fast construction of time- or frequency-domain ROMs. Moreover, we also show that properly constructed RKSs lead to ROMs that preserve general wavefield properties of the unreduced

Manuscript received by the Editor 3 August 2017; revised manuscript received 27 November 2017; published ahead of production 28 December 2017; published online 14 February 2018.
[1]Delft University of Technology, Delft, The Netherlands. E-mail: j.t.zimmerling@tudelft.nl; r.f.remis@tudelft.nl.
[2]Schlumberger-Doll Research, Cambridge, Massachusetts, USA. E-mail: druskin1@slb.com; mzaslavsky@slb.com.

Maxwell system, such as passivity and the Schwarz reflection principle. The order of these rational models is typically much smaller than the order of the ROMs obtained via polynomial or extended Krylov subspace (EKS) methods, but their construction is much more expensive per iteration because it requires the solution of the full (unreduced) discretized Maxwell system at every iteration. ROMs based on RKS techniques are therefore expensive to construct, but they are very efficient to evaluate. This makes them particularly useful in online electromagnetic inversion algorithms, in which only the evaluation of these ROMs is required. Because most applications encountered in geophysics require the computation of wavefield responses in open domains, absorbing boundary conditions have to be included in our Krylov-solution methods. We implement such conditions using complex coordinate stretching techniques and variants thereof (Chew et al., 1997; Druskin and Remis, 2013; Druskin et al., 2016). The implementation of these boundary conditions into the various ROM frameworks is discussed as well. Moreover, we pay particular attention to the effects of the conductivity in the lossy Maxwell system on the convergence speed of the ROMs and illustrate the performance of the various reduction methods by simulating several ground-penetrating radar (GPR) scenarios. Finally, we provide a 3D example using the diffusion approximation of the Maxwell equations and discuss the computational aspect of building the ROMs.

## PROBLEM FORMULATION

We are interested in solving the Maxwell equations:

$$-\nabla \times \mathcal{H} + \sigma \mathcal{E} + \varepsilon \partial_t \mathcal{E} = -\mathcal{J}^{\text{ext}}, \tag{1}$$

$$\nabla \times \mathcal{E} + \mu \partial_t \mathcal{H} = -\mathcal{K}^{\text{ext}}, \tag{2}$$

for one (or multiple) source and receiver locations. In these equations, $\mathcal{E}$ is the electric field strength, $\mathcal{H}$ is the magnetic field strength, and $\sigma$, $\mu$, and $\varepsilon$ are the conductivity, permeability, and permittivity, respectively. The source terms are the electric current density $\mathcal{J}^{\text{ext}}$ and the (equivalent) magnetic current density $\mathcal{K}^{\text{ext}}$. After a finite-difference discretization on a Yee-Lebedev grid, in which we initially set the tangential components of the electric field strength to zero at the outer boundary of the computational domain (perfect electrically conducting [PEC] boundary condition), we obtain the matrix equation

$$\left( \begin{bmatrix} 0 & -\mathsf{D}_{\mathsf{h}} \\ \mathsf{D}_{\mathsf{e}} & 0 \end{bmatrix} + \begin{bmatrix} \mathsf{M}_{\sigma} & 0 \\ 0 & 0 \end{bmatrix} + \begin{bmatrix} \mathsf{M}_{\varepsilon} & 0 \\ 0 & \mathsf{M}_{\mu} \end{bmatrix} \partial_t \right) \begin{bmatrix} \mathsf{e} \\ \mathsf{h} \end{bmatrix} = - \begin{bmatrix} \mathsf{j}^{\text{ext}} \\ \mathsf{k}^{\text{ext}} \end{bmatrix}, \tag{3}$$

where $\mathsf{D}_{\mathsf{h/e}}$ are the finite-difference approximations of the curl operators, $\mathsf{M}_{\varepsilon/\mu/\sigma}$ are the diagonal medium matrices, and $\mathsf{e}$ and $\mathsf{h}$ contain the finite-difference approximations of the electric and magnetic field strength, respectively. Finally, the right side of the above equation contains the finite-difference approximations of the external electric and magnetic current densities. From this moment on, we assume that the time dependence of these densities can be factored out; that is, we consider source vectors of the form $\mathsf{j}^{\text{ext}} = w(t)\mathsf{j}^{\text{sp}}$ or $\mathsf{k}^{\text{ext}} = w(t)\mathsf{k}^{\text{sp}}$, where $\mathsf{j}^{\text{sp}}$ and $\mathsf{k}^{\text{sp}}$ are time independent and $w(t)$ is the source wavelet. Taking $w(t) = \delta(t)$, where $\delta(t)$ is the Dirac distribution operative at $t = 0$, and premultiplying the above equation by

$$\begin{bmatrix} \mathsf{M}_{\varepsilon} & 0 \\ 0 & \mathsf{M}_{\mu} \end{bmatrix}^{-1}, \tag{4}$$

we arrive at a discretized Maxwell system of the form

$$(\mathsf{A} + \partial_t \mathsf{I})\mathsf{u} = \delta(t)\mathsf{b}, \tag{5}$$

where

$$\mathsf{A} = \begin{bmatrix} \mathsf{M}_{\varepsilon} & 0 \\ 0 & \mathsf{M}_{\mu} \end{bmatrix}^{-1} \left( \begin{bmatrix} 0 & -\mathsf{D}_{\mathsf{h}} \\ \mathsf{D}_{\mathsf{e}} & 0 \end{bmatrix} + \begin{bmatrix} \mathsf{M}_{\sigma} & 0 \\ 0 & 0 \end{bmatrix} \right) \tag{6}$$

is our sparse finite-difference Maxwell operator that acts on the fields collected in $\mathsf{u}$, which are excited by the sources in $\mathsf{b}$. Introducing the diagonal step-size matrix $\mathsf{W}_{\mathsf{p}}$ that has the volumes of the primary voxels on its diagonal, the diagonal step-size matrix $\mathsf{W}_{\mathsf{s}}$ with the volumes of the secondary (dual) voxels on its diagonal, and the diagonal matrix

$$\mathsf{W} = \begin{bmatrix} \mathsf{W}_{\mathsf{p}}\mathsf{M}_{\varepsilon} & 0 \\ 0 & -\mathsf{W}_{\mathsf{s}}\mathsf{M}_{\mu} \end{bmatrix}, \tag{7}$$

it can be shown that the Maxwell operator $\mathsf{A}$ satisfies (Remis, 1998)

$$\mathsf{WA} = \mathsf{A}^T\mathsf{W}. \tag{8}$$

This symmetry relation is related to reciprocity. To show this, we first note that equation 5 admits the formal solution

$$\mathsf{u}(t) = \eta(t) \exp(-\mathsf{A}t)\mathsf{b}, \tag{9}$$

where $\eta(t)$ is the Heaviside unit step function. The above solution vector $\mathsf{u}$ contains electric and magnetic field approximations on all grid nodes within the computational domain. In exploration geophysics, however, we are usually not interested in the fields on the entire grid, but only in the transfer function from the sources to the receivers. Introducing a receiver vector $\mathsf{r}$ that selects an electric or magnetic field component at a specific receiver location from the solution vector $\mathsf{u}$, this transfer function is given by

$$\mathsf{f}(\mathsf{r}, \mathsf{b}) = \eta(t)\mathsf{r}^T\mathsf{W} \exp(-\mathsf{A}t)\mathsf{b}. \tag{10}$$

Taking the transpose of this transfer function and using equation 8, it follows that we have the reciprocity relation $\mathsf{f}(\mathsf{r}, \mathsf{b}) = \mathsf{f}(\mathsf{b}, \mathsf{r})$. Finally, we mention that the symmetry properties of equation 5 can also be discussed in terms of the operator $\mathsf{W}^{1/2}\mathsf{A}\mathsf{W}^{-1/2}$ (see, e.g., Remis, 2004).

Because we are mainly interested in electromagnetic fields in open domains, we have to replace the PEC material boundary condition at the outer boundary by an absorbing boundary condition. We implement such a condition by applying coordinate stretching (Chew et al., 1997) in a layer, the perfectly matched layer (PML), which completely surrounds the domain of interest. Because stretching is more easily discussed in the Laplace domain, we continue our analysis in this domain with Laplace parameter $s$. Quantities in the Laplace domain will carry a hat ($\hat{\cdot}$).

Coordinate stretching is introduced by using complex frequency-dependent step sizes $h_i(s) = h_i^{\text{re}} + (h_i^{\text{im}}/s)$ inside the PML, in which the choice for the real and imaginary parts of the step sizes are dependent on the chosen frequency interval. The real part of the

step sizes absorbs evanescent waves, and the imaginary part absorbs propagating waves. The number of complex step sizes needed depends on the frequency interval of interest, the maximum angle of incidence on the PML, and the acceptable reflection coefficients. The desired PML approximates the impedance of infinite half-spaces well over the spectral interval. The impedance of a finite-difference grid with step sized $h_i$ is a rational function, so that the real and imaginary step sizes are obtained from rational approximation of the impedance of an infinite half-space, which permits a closed-form expression (for details, see Druskin et al., 2016). Incorporating this technique leads to a finite-difference operator $\hat{\mathsf{A}}$ that depends on the Laplace parameter $s$, such that equation 5 now reads

$$[\hat{\mathsf{A}}(s) + s\mathsf{I}]\hat{\mathsf{u}} = \mathsf{b}. \tag{11}$$

The symmetry of matrix $\mathsf{A}$ (equation 8) directly translates to the Laplace domain, except that now $\hat{\mathsf{A}}$ and $\hat{\mathsf{W}}$ are $s$ dependent due to the application of the coordinate stretching technique. Explicitly, we have

$$\hat{\mathsf{W}}(s)\hat{\mathsf{A}}(s) = \hat{\mathsf{A}}^T(s)\hat{\mathsf{W}}(s). \tag{12}$$

Furthermore, $\hat{\mathsf{A}}(s)$ follows the Schwarz reflection principle $\hat{\mathsf{A}}(\bar{s}) = \bar{\hat{\mathsf{A}}}(s)$, where the overbar denotes complex conjugation. This principle has to hold because real-valued wavefields (transfer functions) are measured in the time domain. For the inverse Laplace transform of the (Laplace domain) transfer function $\hat{\mathsf{f}}(\mathsf{b},\mathsf{r},s) = \mathsf{r}^T\hat{\mathsf{W}}(s)[\hat{\mathsf{A}}(s) - s\mathsf{I}]^{-1}\mathsf{b}$ to be real valued, it needs to be conjugate symmetric $\bar{\hat{\mathsf{f}}}(\mathsf{b},\mathsf{r},s) = \hat{\mathsf{f}}(\mathsf{b},\mathsf{r},\bar{s})$, and therefore $\hat{\mathsf{A}}(\bar{s}) = \bar{\hat{\mathsf{A}}}(s)$ needs to hold.

Finally, we mention that in the diffusion approximation, that is, when the displacement currents $\epsilon\partial_t\mathcal{E}$ in Maxwell's equations are neglected, we also obtain equation 5 after discretization (see Remis and van den Berg, 1998). In this case, the computational domain can be easily truncated by the PEC material boundary condition at the boundary of the computational domain, provided that this boundary is chosen sufficiently far from the structures of interest. Moreover, in a second-order formulation for diffusion problems, in which one solves for either the electric or the magnetic field strength, the eigenvalues of the resulting discrete diffusion operator lie on the real positive semiaxis, which makes approximation of such an operator fundamentally easier than a wave operator.

### Frequency-independent PML

In our model-order reduction approach, our aim is to approximate the field solution $\hat{\mathsf{u}}(s) = [\hat{\mathsf{A}}(s) + s\mathsf{I}]^{-1}\hat{\mathsf{b}}$ by matrix functions that are easier to compute, for instance, a polynomial or a low-order rational function. However, the introduction of coordinate stretching to simulate open domains results in a discretized Maxwell system that is nonlinear in frequency, which makes it computationally nontractable to build high-order, orthogonal polynomials in $\hat{\mathsf{A}}(s)$ because this requires recompilation of the polynomial for every value of $s$. Therefore, frequency-independent absorbing boundary conditions are desirable. Recent developments in near-optimal PMLs allow for frequency-independent PMLs that are matched over a spectral interval. In these implementations, the spatial step sizes inside the PML are complex and are matched to the temporal spectrum of interest (for details, see Druskin and Remis, 2013; Druskin et al., 2016). This leads to a system of the form

$$(\mathsf{A}^{\mathrm{fi}} + s\mathsf{I})\hat{\mathsf{u}} = \mathsf{b}, \tag{13}$$

where the superscript indicates that frequency-independent coordinate stretching has been implemented using complex spatial step sizes. The above system violates the Schwarz reflection principle as $\hat{\mathsf{u}}(\bar{s}) \neq \bar{\hat{\mathsf{u}}}(s)$ and makes equation 13 unstable because $\mathsf{A}^{\mathrm{fi}}$ has eigenvalues with a negative real part.

However, stable-field approximations can be obtained from equation 13 by computing stability-corrected (Druskin and Remis, 2013; Druskin et al., 2014) transfer functions via

$$\mathsf{f}(\mathsf{r},\mathsf{b}) = 2\eta(t)\mathsf{r}^T\mathsf{W}\,\mathrm{Re}[\eta(\mathsf{A}^{\mathrm{fi}})\exp(-\mathsf{A}^{\mathrm{fi}}t)\mathsf{b}], \tag{14}$$

which also upholds the Schwarz reflection principle in the Laplace domain because

$$\begin{aligned}\hat{\mathsf{f}}(\mathsf{r},\mathsf{b}) = {} & \mathsf{r}^T\mathsf{W}\eta(\mathsf{A}^{\mathrm{fi}})(\mathsf{A}^{\mathrm{fi}} + s\mathsf{I})^{-1}\mathsf{b} \\ & + \mathsf{r}^T\mathsf{W}\eta(\overline{\mathsf{A}^{\mathrm{fi}}})(\overline{\mathsf{A}^{\mathrm{fi}}} + s\mathsf{I})^{-1}\mathsf{b}.\end{aligned} \tag{15}$$

Here, $\eta(z)$ is the Heaviside unit-step function acting on the real part of its argument, such that $\eta(\mathsf{A}^{\mathrm{fi}})$ is a projector onto the stable part of our finite-difference matrix. By fixing the PML frequency to a positive imaginary Laplace frequency, the matrix $\mathsf{A}^{\mathrm{fi}}$ has stable eigenvalues in the quadrant $\mathrm{Re}(s) > 0$ and $\mathrm{Im}(s) > 0$, and it has unstable eigenvalues in the quadrant $\mathrm{Re}(s) < 0$ and $\mathrm{Im}(s) < 0$. The unstable eigenvalues correspond to incoming wavefields for a frequency $\mathrm{Im}(s) < 0$ because the fixed frequency PML fails to approximate the sign change in the radiation condition as $\mathrm{Im}(s)$ changes sign. However, the projector $\eta(\mathsf{A}^{\mathrm{fi}})$ allows us to obtain the stable part of the operator and the Schwarz reflection principle allows us to find a stable transfer function valid for all Laplace parameters $s$ with $\mathrm{Re}(s) > 0$.

To summarize, the frequency-independent PML formulation described above linearizes equation 11 with respect to frequency (see equation 13), but it requires stability correction as described in equations 14 and 15. This stability-correction approach works in general, but, as we will show in the next section, it is not always necessary. Specifically, in configurations in which it is sufficient to approximate $\hat{\mathsf{u}}$ by a low-order rational function, a frequency-dependent PML can be used because the construction of such a function only requires solutions of equation 11 for a small number of different frequencies.

## REDUCED-ORDER MODELING

The finite-difference system of equation 11 is large for real-world applications and obtaining a time-domain or frequency-domain solution over a frequency interval of interest can be too cumbersome. In reduced-order modeling, we therefore approximate the wavefield in terms of a small basis, to reduce the order of the systems of equations that need to be solved.

## Structure-preserving rational Krylov subspace approximations

Let us start with the construction of the RKS-ROMs, formally introduced for eigenvalue problems by Ruhe and Skoogh (1998). These approximations are constructed out of field solutions of the discretized Maxwell system at particular frequencies $s = \kappa_1$, $s = \kappa_2$, $\ldots$, $s = \kappa_m$. Note that a rational Krylov method has no problem in handling the nonlinear dependence of $\hat{\mathsf{A}}$ on $s$ because the subspace is spanned by single-frequency solutions to the problem.

As a first step, we multiply equation 11 by the frequency-dependent and nonsingular step size matrix $\hat{\mathsf{W}}(s)$ to obtain the system

$$\hat{\mathsf{B}}(s)\hat{\mathsf{u}}(s) = \mathsf{b}', \tag{16}$$

where $\hat{\mathsf{B}}(s) = \hat{\mathsf{W}}(s)[\hat{\mathsf{A}}(s) + s\mathsf{I}]$. The sources $\mathsf{b}$ are supported outside the PML, and thus inside the computational domain of interest. The step sizes contained in the step-size matrix $\hat{\mathsf{W}}(s)$ are frequency dependent inside the PML only, so that the product $\mathsf{b}' = \hat{\mathsf{W}}(s)\mathsf{b}$ is frequency independent. Note that $\hat{\mathsf{B}}(s)$ is symmetric because of equation 12. As a next step, we solve equation 16 at the $m$ different frequencies $s = \kappa_1, s = \kappa_2, \ldots, s = \kappa_m$ to obtain the corresponding solutions $\hat{\mathsf{u}}(\kappa_1)$, $\hat{\mathsf{u}}(\kappa_2)$, $\ldots$, $\hat{\mathsf{u}}(\kappa_m)$. Subsequently, we use these solutions to construct our rational Krylov ROMs. This RKS deviates from the classical definition because the operator used to construct it is frequency dependent. We would like the reduced-order model to preserve the symmetry, passivity, and Schwarz reflection principle of the full-order model, to honor the underlying physics. To this end, the set of interpolation points needs to be closed under conjugation; that is, the complex conjugate of the set of interpolation points lies within the set of interpolation points itself. With $\kappa = \{s_1, s_2, \ldots, s_m\}$ and choosing $\kappa \cup \bar{\kappa}$ as the set of interpolation points, the RKS itself is closed under conjugation and contains the solutions $\hat{\mathsf{u}}(\kappa_j)$ and $\hat{\mathsf{u}}(\bar{\kappa_j}) = \overline{\hat{\mathsf{u}}(\kappa_j)}$. This can be achieved by choosing the real, structure-preserving RKS of size $2m$

$$\begin{aligned}\mathcal{K}^{2m}_{\mathrm{RKS}} = \mathrm{span}\{&\mathrm{Re}\,\hat{\mathsf{u}}(\kappa_1), \mathrm{Im}\,\hat{\mathsf{u}}(\kappa_1), \ldots,\\ &\ldots, \mathrm{Re}\,\hat{\mathsf{u}}(\kappa_m), \mathrm{Im}\,\hat{\mathsf{u}}(\kappa_m)\},\end{aligned} \tag{17}$$

as an approximation and a weighting space for the construction of the RKS-ROMs. Although the subspace has a dimension of $2m$, only $m$ single-frequency solutions are required and the required memory for storing the basis is equivalent to storing $m$ complex vectors.

To construct the RKS-ROMs, let $\mathsf{V}_m \in \mathbb{R}^{N\times 2m}$ span the subspace $\mathcal{K}^{2m}_{\mathrm{RKS}}$ and write the ROM solution as $\hat{\mathsf{u}}_m(s) = \mathsf{V}_m\hat{\mathsf{y}}_m(s)$, where $\hat{\mathsf{u}}_m(s)$ is a vector containing the $2m$ $s$-dependent expansion coefficients. The residual that corresponds to this approximation is given by $\hat{\mathsf{r}}(s) = \mathsf{b}' - \hat{\mathsf{B}}(s)\hat{\mathsf{u}}_m(s)$ and by requiring that this residual is orthogonal to $\mathsf{V}_m \in \mathbb{R}^{N\times 2m}$ (Galerkin condition), the RKS-ROM follows as

$$\hat{\mathsf{u}}_m(s) = \mathsf{V}_m[\mathsf{V}_m^T\hat{\mathsf{B}}(s)\mathsf{V}_m]^{-1}\mathsf{V}_m^T\mathsf{b}', \tag{18}$$

where the inverse in the above expression exists for all frequencies $\mathrm{Re}(s) \geq 0$ of interest because the projection is structure preserving. The reduced-order matrix $\mathsf{V}_m^T\hat{\mathsf{B}}(s)\mathsf{V}_m$ preserves the symmetry of the problem, and even passivity because $\mathsf{V}_m$ is real. More specifically, the (nonlinear) numerical range of the projected system

$$\mathcal{N}\{\mathsf{V}_m^T\hat{\mathsf{B}}(s)\mathsf{V}_m\} = \{s \in \mathbb{C} : \hat{\mathsf{x}}^H\mathsf{V}_m^T\hat{\mathsf{B}}(s)\mathsf{V}_m\hat{\mathsf{u}} = 0;\ \ \forall\,\hat{\mathsf{u}} \in \mathbb{C}\setminus 0\} \tag{19}$$

lies within the numerical range of the full operator $\mathcal{N}\{\hat{\mathsf{B}}(s)\}$. This implies that if the full-order system is passive, so is the reduced-order system. Passive systems do not produce any energy, so that the energy in the system is smaller or equal to the energy fed into the system. Strictly passive systems dissipate the input energy (Sorensen, 2003). Thus, passive systems are by definition stable. Furthermore, the reduced-order solution $\hat{\mathsf{u}}_m$ interpolates the full solution $\hat{\mathsf{u}}$ at all Laplace frequencies $\kappa_i$ and $\bar{\kappa}_i$. This follows from the uniqueness of the Galerkin condition and from the fact that the fields $\hat{\mathsf{u}}(\kappa_i)$ and $\hat{\mathsf{u}}(\bar{\kappa}_i)$ are in the RKS.

## Polynomial and extended Krylov methods

Polynomial and extended Krylov ROMs can be constructed for frequency-independent PML formulations (on a frequency interval of interest because these methods cannot directly handle the nonlinear dependence of the discretized Maxwell operator on the frequency). Therefore, we take equation 13 as a starting point and exploit the fact that matrix $\mathsf{A}^{\mathrm{fi}}$ is symmetric with respect to the diagonal, nonsingular, frequency-independent, and complex step-size matrix $\mathsf{W}$ to construct a basis of the polynomial Krylov subspace (PKS)

$$\mathcal{K}^m_{\mathrm{PKS}} = \mathrm{span}\{\mathsf{b}, \mathsf{A}^{\mathrm{fi}}\mathsf{b}, \ldots, (\mathsf{A}^{\mathrm{fi}})^{m-1}\mathsf{b}\}, \tag{20}$$

via a modified three-term Lanczos algorithm (Jea and Young, 1983; Freund and Nachtigal, 1995). This subspace can now be used to obtain polynomial, stability-corrected Krylov subspace approximations for the transfer functions (Druskin and Remis, 2013). Similarly, the $\mathsf{W}$-symmetry of $\mathsf{A}^{\mathrm{fi}}$ can be exploited to efficiently construct a basis of the EKS

$$\mathcal{K}^{n_{\mathrm{n}},n_{\mathrm{p}}}_{\mathrm{EKS}} = \mathrm{span}\{(\mathsf{A}^{\mathrm{fi}})^{-n_{\mathrm{n}}}\mathsf{b}, \ldots, \mathsf{b}, \ldots, (\mathsf{A}^{\mathrm{fi}})^{n_{\mathrm{p}}-1}\mathsf{b}\}, \tag{21}$$

via a five-term recurrence relation (Jagels and Reichel, 2011) and extended Krylov transfer function approximations can efficiently be computed (Druskin et al., 2014). The short recursion relations together with the fact that only the transfer function

$$\mathsf{f}(\mathsf{r},\mathsf{b}) = \mathsf{r}^T\mathsf{W}g(\mathsf{A}^{\mathrm{fi}})\mathsf{b} \tag{22}$$

is needed rather than the whole field approximation allows for the computation of the transfer function without storing the basis. Here, $g(\cdot)$ is the (stability corrected) exponential for time-domain and the resolvent for frequency-domain problems (see equations 14 and 15). With $\mathsf{V}_m \in \mathbb{C}^{N\times m}$ as the basis for the PKS or EKS ($m = n_n + n_p$), the reduced-order transfer function can be written as

$$\mathsf{f}_m(\mathsf{r},\mathsf{b}) = \mathsf{r}^T\mathsf{W}\mathsf{V}_m g(\mathsf{V}_m^H\mathsf{W}\mathsf{A}^{\mathrm{fi}}\mathsf{V}_m)\mathsf{V}_m^H\mathsf{W}\mathsf{b}, \tag{23}$$

using short-term recurrence algorithms. Because the projection of the operator is computed within the short-term recurrence algorithm, only the inner products $\mathsf{r}^T\mathsf{W}\mathsf{V}_m$ and $\mathsf{V}_m^H\mathsf{W}\mathsf{b}$ need to

be kept in memory and the basis does not need to be stored. The projected Maxwell operator $\mathsf{V}_m^H\mathsf{W}\mathsf{A}^{\text{fi}}\mathsf{V}_m$ is tridiagonal for PKS and pentadiagonal in the case of EKS, further simplifying the evaluation of $g(\mathsf{V}_m^H\mathsf{W}\mathsf{A}^{\text{fi}}\mathsf{V}_m)$. Adding a vector to a PKS is computationally cheap and just requires one matrix vector multiplication: It is equivalent to one finite-difference time-domain (FDTD) step in cost. However, adding a negative power of matrix $\mathsf{A}^{\text{fi}}$ to an EKS is computationally more expensive because one has to numerically solve a static (zero frequency) problem. Generally, EKS performs well if low frequencies need to be approximated, as it interpolates the original function and its first $n_n - 1$ derivatives at the zero frequency. Finally, we mention that polynomial and extended Krylov field approximations of the stability-corrected transfer function are stable by construction because all eigenvalues of $\eta(\mathsf{A}^{\text{fi}})$ and $\eta(\overline{\mathsf{A}^{\text{fi}}})$ lie in the right half-plane.

The matrix $\mathsf{A}^{\text{fi}}$ is singular for wave propagation and diffusion, and we therefore need to solve the system with the pseudoinverse of $\mathsf{A}^{\text{fi}}$ (Remis, 2004). In the case of 2D wave propagation, this pseudoinverse corresponds to the law of Biot-Savart (the action of $\mathsf{A}^{\text{fi};\dagger}\mathsf{b}$). One has to essentially solve the Poisson's equations to compute the action of the pseudoinverse on a right side (Druskin and Knizhnerman, 1998). This can be done with standard Poisson's solvers or more generally with iterative solvers computing the minimum norm solution. Finally, we mention that in our model-reduction approach, we approximate shifted systems using polynomial and extended Krylov subspaces. The first-order Maxwell system leads to such a linear system if a fixed-frequency PML is used. The second-order Maxwell system leads to a quadratic equation

$$(\mathsf{D} + \mathsf{M}_{\varepsilon\mu}s^2 + \mathsf{M}_{\mu\sigma}s)\mathsf{e} = \mathsf{b} \tag{24}$$

that can only be viewed as a shifted system in the lossless case, in the diffusion approximation, or if $\varepsilon$ is proportional to $\sigma$ throughout the domain (see Remis, 1998). Thus, for general lossy Maxwell systems, the first-order formulation is used in the proposed approach.

## DIFFUSION APPROXIMATION VERSUS FULL MAXWELL SYSTEM

For the Maxwell equations in the diffusion approximation, polynomial or rational Krylov subspace clearly outperform time-stepping schemes (Druskin and Knizhnerman, 1994; Knizhnerman et al., 2009; Börner et al., 2015). In particular, to obtain the time-domain solution in the interval $[0, T]$ to the diffusion equations discretized with step size $h$, one needs $m = \mathcal{O}(h^{-1}\sqrt{\log(h)T})$ PKS iterations as opposed to $\mathcal{O}(h^{-2}T)$ time steps using an explicit second-order time-stepping scheme. Furthermore, the eigenvalues of the diffusion operator lie on the positive, real semiaxis so that the optimal shifts for an RKS are known via a Zolotarev rational approximant (Knizhnerman et al., 2009). In contrast, the Courant–Friedrichs–Lewy condition of the FDTD method for Maxwell's wave equations with lossless media yields an estimate of only $\mathcal{O}(h^{-1}T)$ time steps. In fact, one can show that the PKS method for these types of problems is computationally equivalent to FDTD with an optimal time step in case of PEC boundary conditions and lossless media (Remis, 2011). Material losses and the PML, however, shift the spectrum of the first-order wave operator away from the imaginary axis and into the complex plane. The separation of the spectrum from the area of approximation (the imaginary axis) enhances the convergence of PKS.

In Figure 1, we show the spectrum of a typical discretized first-order wave and second-order diffusion operator. All eigenvalues are shown as red crosses and are located in the right half of the complex $s$-plane. The spectra of the diffusion and wave operator are clearly different — eigenvalues of the diffusion operator are located on the positive real line, whereas the wave operator has a (symmetric) spectrum that is completely located in the stable right half-plane $\text{Re}(s) \geq 0$. For frequency-domain problems, we want to obtain an accurate approximation in a frequency interval of interest that is usually located on the imaginary axis (encircled with a dashed black line). After discretization of the continuous wave operator, its spectrum becomes discrete and shifts into the complex plane due to material losses and the introduction of a PML. The fixed-frequency PML is only matched in a certain region of interest, corresponding to strongly damped eigenvalues with a large real part. Cavities or other resonant inclusions can introduce so-called resonance modes, which are characterized by eigenvalues with a small real part because they lead to a slowly decaying exponent in the transfer function of equation 14. The separation of the area of approximation and the spectrum also allows for efficient model reduction via RKS. However, contrary to the diffusive case, the eigenvalues of the wave operator are not located on the real axis, but they can be found in the complex plane (for more information about the spectrum of $\hat{\mathsf{A}}(s)$, we refer to Kim and Pasciak [2009], for example). A priori selection of optimal shifts as in the diffusive case is therefore very difficult. In general, the frequency-domain response of a wave equation can be oscillatory, which limits an interpolatory method such as the RKS method. In conclusion, introducing losses into the Maxwell system allows us to find smaller reduced-order models. Losses lead to a loss of information and allow for a low-order approximation that can capture the relevant features of the transfer function. This will be illustrated with a numerical experiment in the "Results" section.

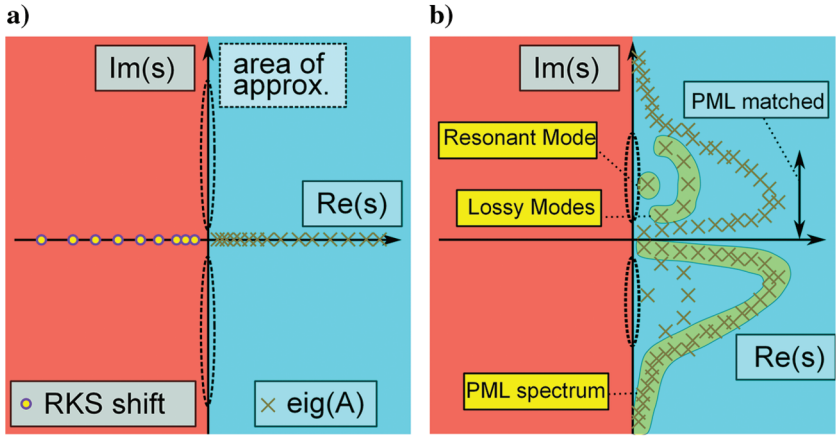


Figure 1. Illustration of the eigenvalues of (a) the second-order diffusion operator and (b) the (linearized) first-order wave operator $\mathsf{A}^{\text{fi}}$, including stability correction. The unstable left half-plane ($\text{Re}(s) < 0$) is depicted in red, whereas the stable right half-plane ($\text{Re}(s) > 0$) is shown in blue.

## RESULTS

In this section, we use several GPR scenarios to illustrate the performance of the various Krylov reduction techniques. In addition, a 3D example for the diffusive Maxwell equations is presented as well, and we conclude the "Results" section by a discussion of the computational aspect of the introduced methods.

### 2D GPR

To show the approximation qualities of the introduced ROMs, we consider a configuration arising in exploration with GPR. We investigate a lossy subsurface with a box-shaped anomaly, and we use a frequency band between 50 MHz and 3 GHz. The simulated configuration is shown in Figure 2, in which the exact medium parameters are provided in the caption. An electrical dipole source oriented in the $z$-direction is used for excitation, and the $z$-component of the electric field strength is measured at the ground-air interface. Finite-difference discretization with a second-order accurate operator and eight points per smallest wavelength at 3 GHz leads to a first-order Maxwell system with $N = 62 \times 10^3$ unknowns. Using this full operator, we compute the transfer function for this configuration using an FDFD method to obtain a comparison solution for our reduced-order models. This comparison solution is shown alongside the responses of the PKS, EKS, and RKS reduced-order models in Figure 3. The order of the reduced-order models was increased until the reduced-order models and the comparison solution essentially overlap on the frequency interval of interest.

For the RKS method, we choose equidistant shifts (interpolation points) on the imaginary axis between 50 MHz and 3 GHz. The RKS method leads to the smallest model with $m = 55$; however, a single iteration is much more expensive than a PKS iteration. The PKS method needs $m = 3400$ iterations until convergence,

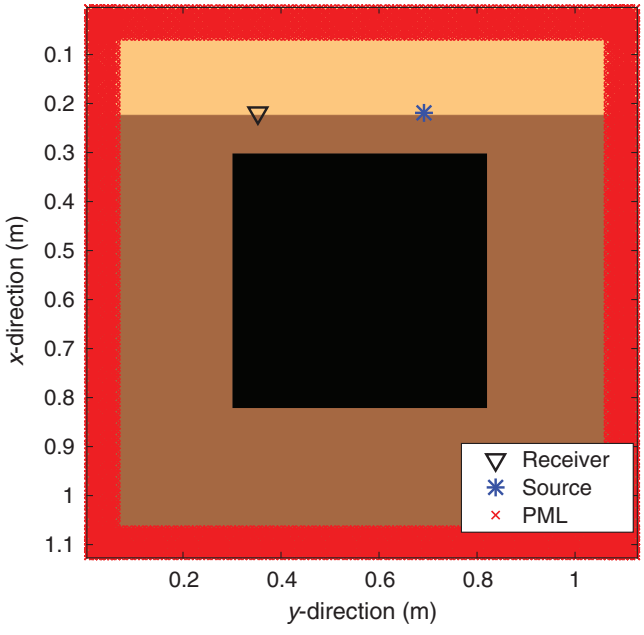


Figure 2. Simulated GPR configuration, with an ($\varepsilon_r = 4$, $\sigma = 10^{-2}$ S/m) anomaly embedded in a ($\varepsilon_r = 2, \sigma = 5 \times 10^{-4}$ S/m) surface layer, with dry air $\varepsilon_r = 1, \sigma = 0$ on top.

where one iteration is as expensive as an FDTD step. The EKS method needs $n_n = 100$ inverse and $n_p = 2200$ forward iterations. The only difference can be seen at very low frequencies where the frequency-independent and -dependent PML deviate. Furthermore, the PKS method converges from large eigenvalues toward small eigenvalues, meaning that high frequencies are approximated first. The EKS method with 100 inverse iterations interpolates at the zero frequency such that it converges from low and high frequencies toward the middle spectrum. The RKS method with uniform distributed shifts interpolates the response at all shifts, and it therefore converges on the whole interval of shifts simultaneously. The convergence of the different Krylov methods in the frequency domain is shown in more detail in Figure 4, in which the relative $L_2$-error between the different Krylov ROMs and the FDFD comparison solution is shown as a function of the number of iterations. We measure the approximation by the relative $L_2$-error in the time domain

$$\text{err} = \frac{\|\mathbf{f}_m(t) - \mathbf{f}(t)\|_2}{\|\mathbf{f}(t)\|_2}, \tag{25}$$

and we use an FDFD comparison simulation to obtain $\mathbf{f}(t)$.

The RKS-ROM converges up to machine precision to the FDFD comparison solution because both solutions are computed using the frequency-dependent Maxwell operator. The error of the PKS and EKS ROMs stagnates at around an error level of approximately $10^{-4}$ because these models use the frequency-independent PML formulation.

The convergence of the PKS method in the time domain is illustrated in Figure 5. Here, the time derivative of a Gaussian pulse, shifted to 1.15 GHz, was used as a wavelet. The 1% cut-off frequency of this wavelet is 2.4 GHz, and discretization is chosen such that we have approximately 10 points per the smallest wavelength at this cut-off frequency. We observe that early times are approximated well after $m = 1100$; however, late times containing the reflection of the anomaly did not yet converge. After $m = 3400$ iterations, the

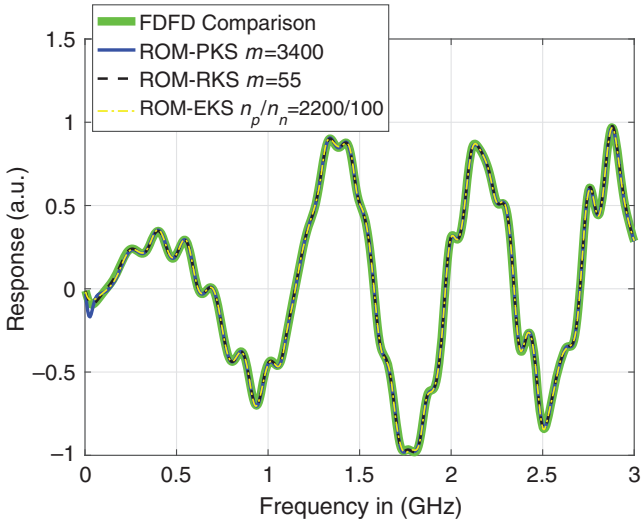


Figure 3. Imaginary part of the transfer function over the frequency interval of interest computed with FDFD (solid green line), PKS after 3400 iterations (solid blue line), EKS after 2200 forward and 100 inverse iterations with $\mathbf{A}^{\text{fi}}$, respectively, (solid yellow line), and RKS after 55 iterations (dashed line).

time-domain error is less than 0.1% and the reduced-order approximation and FDFD comparison solution are indistinguishable. The direct arrival of the pulse and the reflections from the anomaly can clearly be distinguished in this experimental setup.

To study the effect of losses on the convergence rate of RKS-ROMs in the time domain, we repeat the above experiment with different conductivity models. Specifically, we scale the conductivity profile by factors of 0.5, 2, and 5. The relative time-domain errors (with respect to an FDTD comparison solution) for different iterations of RKS are shown in Figure 6, in which we used the same wavelet as in the previous experiment. Higher losses clearly increase the convergence rate because it shifts the spectrum of the operator further away from the imaginary axis and into the complex plane. For small dimensions of the Krylov subspace, the errors in all experiments are similar due to the presence of a direct lossless path between the sources and receivers. Once this direct arrival is well-approximated, the errors of the different conductivity models start to differ and higher losses positively influence the convergence rate. The convergence of RKS is not monotonic, however, because we use equidistant shifts for our experiments, meaning that we rebuild our subspace for each of the experiments.

## 3D electromagnetic diffusion

In case the displacement currents $\epsilon\partial_t\mathcal{E}$ are negligible compared with the conduction currents, we obtain the diffusion approximation of the Maxwell's equations. In this computational example, we consider a 3D configuration with a resistive, anisotropic anomaly. The geometric configuration is a scaled version of the previous example, and it is shown in Figure 7, in which the source and receiver are directed in the positive $y$-direction. The lower half-space has conductivity of $\sigma = 1$ S/m, and the resistive, anisotropic, cube anomaly has principal components of $\sigma_{\mathrm{I}} = 0.01$ S/m, $\sigma_{\mathrm{II}} = 0.04$ S/m, and $\sigma_{\mathrm{III}} = 0.02$ S/m with a dip and azimuth angle of the anisotropy of 30° and 15°. After discretization with finite differences, the model has $N = 1.5 \times 10^6$ field unknowns in a second-order formulation.

The interpolation points of the RKS method are placed on the negative real semiaxis and chosen asymptotically optimal assuming a uniform spectral distribution of the diffusion operator, as described by Druskin et al. (2009). Therefore, the shifts are known a priori and the dimension of the RKS can be increased by adding vectors one by one.

In Figure 8a, the $L_2$-error of the ROM is shown as a function of the iteration number $m$ for the PKS and RKS methods. Both methods converge to a relative error of $10^{-4}$ in $m_{\mathrm{PKS}} = 18{,}700$ and $m_{\mathrm{RKS}} = 33$ iterations, respectively. To show the convergence within a single figure, double logarithmic axes are used. The RKS method clearly yields a smaller ROM.

The wall times for a sequential implementation are shown in Figure 8b, the RKS method clearly outperforms the PKS method in terms of computation time and size of the ROM. However,

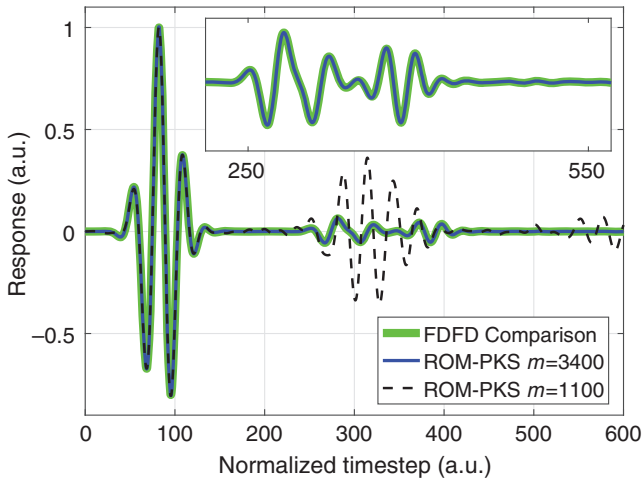


Figure 5. Time-domain trace as approximated by the PKS method after 1100 iterations and 3400 iterations. For a PKS method, the early times converge first. The reflections from the anomaly can be seen in the magnified panel in the top right. The FDTD comparison response and ROM-PKS response for $m = 3400$ are magnified for (normalized) times between 250 and 550.

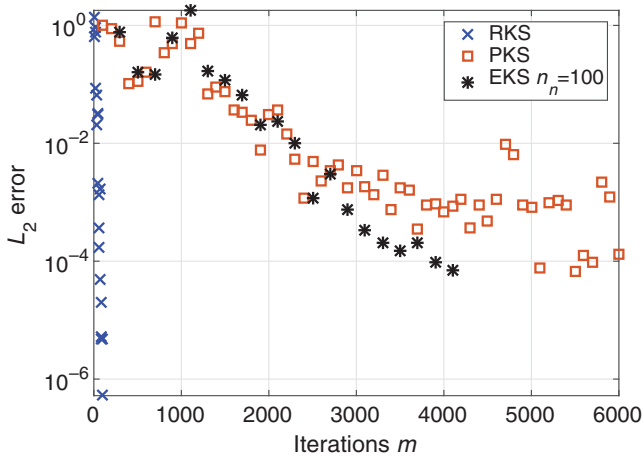


Figure 4. Relative error of the PKS, EKS, and RKS-ROMs. The PKS and EKS-ROMs stagnate around a relative error of approximately err $= 10^{-4}$, as the comparison solution was computed with an FDFD method with frequency-dependent PML.

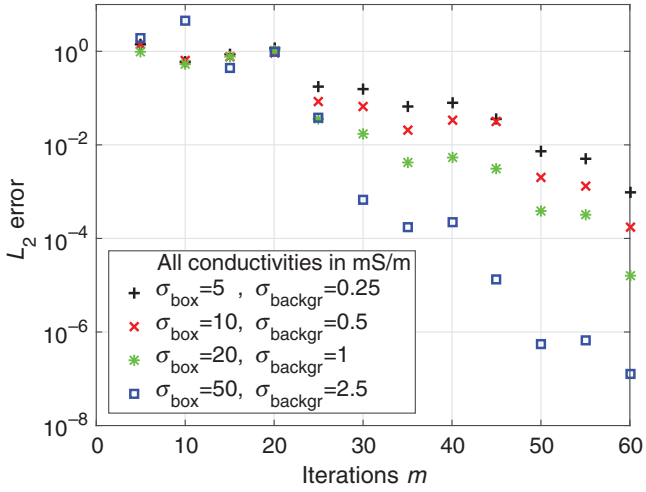


Figure 6. Time-domain convergence of the RKS method for four different media. All conductivities are given in mS/m, and the red crosses correspond to the previously discussed experiment.

the PKS method uses less memory to construct the ROM. In the next section, we discuss the computational complexity of the ROM methods in more detail. We choose to show the wall times in a semilogarithmic scale and the $L_2$-error as function of the iterations on a double logarithmical scale because the asymptotic complexity of a single iteration of RKS is constant, so is the complexity of PKS.

The time-domain transfer function as approximated by the RKS and PKS methods for the time interval of interest ($t = 10^{-3}$–$10^{-1}$ s) is shown in Figure 9. A slight difference at early times between these methods is caused by the different averaging techniques used in RKS and PKS for spatial discretization (see nodal homogenization and standard homogenization, respectively, from Moskow et al., 1999). In this experiment, a Heaviside step function is used as a wavelet that is active for all negative times and zero for all positive times (switch-off source). The observed $L_2$-error between both methods for the time trace shown in Figure 9 is 3%.

## Discussion on computational complexity

In this section, we briefly discuss the computational complexity and memory requirements of the PKS, EKS, and RKS algorithms. With $N$ denoting the order of the original unreduced Maxwell system and $m$ denoting the order of the ROM, the performance of all three methods can be summarized as in Table 1. From this table, it is clear that there is a tradeoff between memory requirements and computational complexity. Specifically, one iteration of RKS is much more costly than one iteration of PKS or EKS because it requires a solution of the unreduced Maxwell system at each iteration. On the other hand, RKS typically converges much faster than does PKS or EKS, as demonstrated in the numerical results section. Another advantage of the RKS method is that the construction

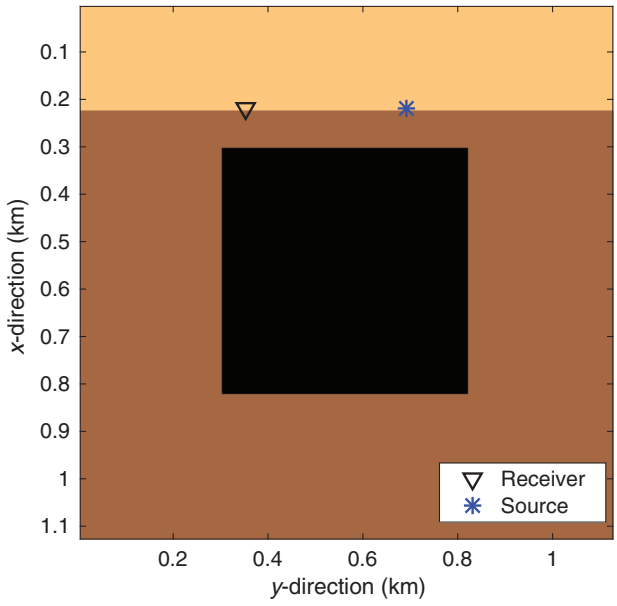


Figure 7. Cross section of the 3D model simulated with a lower half-space of $\sigma = 1$ S/m and a lossless upper half-space. A resistive, anisotropic, cube anomaly with principal components of $\sigma_{\mathrm{I}} = 0.01$ S/m, $\sigma_{\mathrm{II}} = 0.04$ S/m, and $\sigma_{\mathrm{III}} = 0.02$ S/m is present in the configuration. The dip and azimuth of the anisotropy are 30° and 15°, respectively.

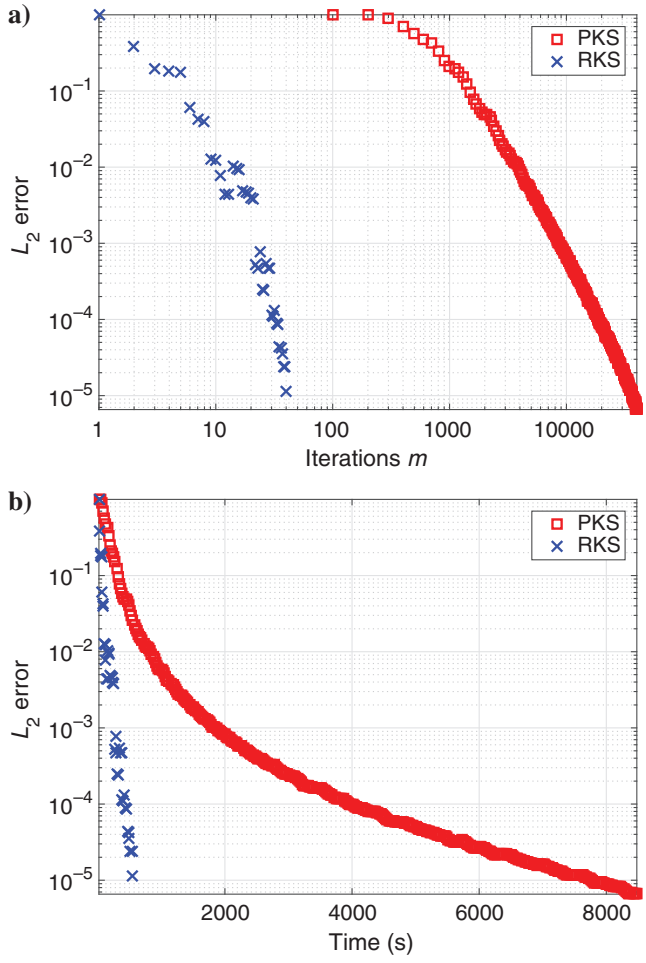


Figure 8. (a) Time-domain error of the RKS and PKS reduced-order models as a function of the iteration number $m$ shown on a log-log scale. (b) Time-domain error of the RKS and PKS reduced-order model for a given computation time.

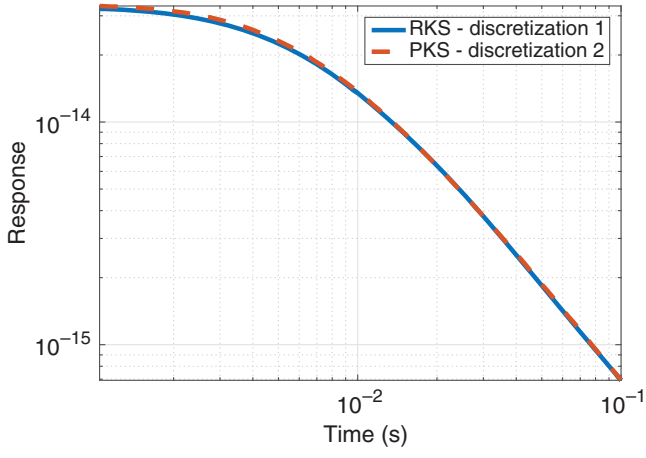


Figure 9. Time-domain response for the converged RKS and PKS reduced-order models. To estimate the error introduced by finite-difference discretization, the PKS and RKS methods use different homogenization methods.

**Table 1. Computational complexity, memory requirement, and possible parallelization of the PKS, RKS, and EKS methods.**

| Method | Asymptotic complexity | Memory | Possible parallelization |
|---|---|---|---|
| RKS | $\phi(N)Nm$ | $mN$ | $m$ |
| PKS | $Nm$ | $3N$ | — |
| EKS | $\varphi(N)Nm$ | $5N$ | — |

$\phi(N)N$ — complexity of solving one shifted system.
$\varphi(N)N$ — complexity of solving one static system ($s = 0$).

of the RKS basis is parallelizable as multiple shifted systems can be solved in parallel. From a memory point of view, the PKS and EKS algorithms are more attractive due to the short-term recurrence relations that allow for a memory-efficient construction of these spaces. Only three vectors of the size of the computational domain need to fit the computational memory for PKS and five vectors for EKS. For the RKS method, $m$ vectors need to be stored in memory. Finally, we note that in a sequential implementation of the RKS and PKS method, the computational cost of each iteration of RKS or PKS is approximately constant. Our 3D diffusive example showed, however, that the convergence of PKS slows down as the error decreases, whereas the RKS shows linear convergence and RKS outperforms PKS in terms of computation time (see also Figure 8b).

## CONCLUSION

In this paper, we have presented polynomial, extended, and rational Krylov reduced-order modeling techniques for the Maxwell equations on open domains. The model-reduction techniques have been applied to a GPR configuration, involving lossy media and an anisotropic diffusion configuration. Polynomial and extended ROMs are based on a frequency-independent PML formulation in combination with a stability-correction procedure to obtain accurate transfer function approximations between a given source and a given receiver. By exploiting the symmetry of Maxwell's equations, we have shown that PKS- and EKS-ROMs can be constructed using short recurrence relations and it is not necessary to store a complete Krylov basis to evaluate transfer function approximations for the fields.

Constructing PKS- and EKS-ROMs can be realized at low computational cost, but the order of these models can be much larger than the order of the RKS models. This makes PKS and EKS particularly well-suited for online field computations. RKSs, on the other hand, generally yield the smallest models; however, for some applications and configurations, the low cost of a single iteration of PKS or EKS outweighs this advantage. Furthermore, generating an RKS demands more memory because we have to save the basis. However, if the goal is to obtain a reduced-order model of the smallest order and this model can be computed offline, then RKS-ROMs may be preferred. Another advantage of an RKS approach over PKS- and EKS-ROM construction is that it does not require linearization of the PML and a stability-correction procedure is not necessary.

What all methods have in common is that the convergence rate of the models improves as the losses within the configuration increase. When solving wavefield problems on open domains, PMLs that simulate outward wave propagation automatically introduce a loss mechanism into the system that moves the spectrum of the first-order Maxwell wave operator away from the imaginary axis, where the wavefield responses are approximated. If, in addition, material losses are present as well, the spectrum moves away even further into the complex frequency plane and this separation increases as the loss profiles of the different media increase. This separation has a positive effect on the convergence rate of the Krylov ROMs, and lower-order models are sufficient to accurately model the transfer function responses between a source and a receiver. Physically, an increase in conductivity leads to a loss of information and smoother wave responses, which can be more easily approximated, resulting in ROMs of a lower order.

Finally, for Maxwell's equations in the diffusion approximation, rational approximation of the transfer function via RKS is clearly superior in computation time and the resulting model order. The separation of the spectrum and the area of approximation are intrinsic to the problem in this case, and optimal shifts for RKS can be found.

## ACKNOWLEDGMENTS

The research presented in this paper was financially supported by the Dutch technology foundation Stichting voor de Technische Wetenschappen (project number 14222). This support is gratefully acknowledged. We thank the reviewers for their helpful comments and suggestions to improve this manuscript. We also gratefully acknowledge the support of Institute for Computational and Experimental Research in Mathematics during the preparation of this manuscript.

## REFERENCES

Antoulas, A., 2005, Approximation of large-scale dynamical systems: SIAM.
Benner, P., S. Gugercin, and K. Willcox, 2015, A survey of projection-based model reduction methods for parametric dynamical systems: SIAM Review, **57**, 483–531, doi: 10.1137/130932715.
Borcea, L., V. Druskin, A. V. Mamonov, and M. Zaslavsky, 2014, A model reduction approach to numerical inversion for a parabolic partial differential equation: Inverse Problems, **30**, 125011, doi: 10.1088/0266-5611/30/12/125011.
Börner, R.-U., O. G. Ernst, and S. Güttel, 2015, Three-dimensional transient electromagnetic modeling using rational Krylov methods: Geophysical Journal International, **202**, 2025–2043, doi: 10.1093/gji/ggv224.
Budko, N. V., and R. F. Remis, 2004, Electromagnetic inversion using a reduced-order three-dimensional homogeneous model: Inverse Problems, **20**, S17–S26, doi: 10.1088/0266-5611/20/6/S02.
Chew, W. C., J. M. Jin, and E. Michielssen, 1997, Complex coordinate stretching as a generalized absorbing boundary condition: Microwave and Optical Technology Letters, **15**, 363–369, doi: 10.1002/(ISSN)1098-2760.
Druskin, V., S. Güttel, and L. Knizhnerman, 2016, Near-optimal perfectly matched layers for indefinite Helmholtz problems: SIAM Review, **58**, 90–116, doi: 10.1137/140966927.
Druskin, V., and L. Knizhnerman, 1994, Spectral approach to solving three-dimensional Maxwell's diffusion equations in the time and frequency domains: Radio Science, **29**, 937–953, doi: 10.1029/94RS00747.
Druskin, V., and L. Knizhnerman, 1998, Extended Krylov subspaces: Approximation of the matrix square root and related functions: SIAM Journal on Matrix Analysis and Applications, **19**, 755–771, doi: 10.1137/S0895479895292400.
Druskin, V., L. Knizhnerman, and M. Zaslavsky, 2009, Solution of large scale evolutionary problems using rational Krylov subspaces with optimized shifts: SIAM Journal on Scientific Computing, **31**, 3760–3780, doi: 10.1137/080742403.
Druskin, V., and R. F. Remis, 2013, A Krylov stability-corrected coordinate-stretching method to simulate wave propagation in unbounded domains: SIAM Journal on Scientific Computing, **35**, B376–B400, doi: 10.1137/12087356X.

Druskin, V., R. F. Remis, and M. Zaslavsky, 2014, An extended Krylov subspace model-order reduction technique to simulate wave propagation in unbounded domains: Journal of Computational Physics, **272**, 608–618, doi: 10.1016/j.jcp.2014.04.051.

Druskin, V., and M. Zaslavsky, 2007, On combining model reduction and Gauss-Newton algorithms for inverse partial differential equation problems: Inverse Problems, **23**, 1599–1610, doi: 10.1088/0266-5611/23/4/013.

Freund, R., and N. Nachtigal, 1995, Software for simplified Lanczos and QMR algorithms: Applied Numerical Mathematics, **19**, 319–341, doi: 10.1016/0168-9274(95)00089-5.

Jagels, C., and L. Reichel, 2011, Recursion relations for the extended Krylov subspace method: Linear Algebra and its Applications, **434**, 1716–1732, doi: 10.1016/j.laa.2010.08.042.

Jea, K. C., and D. M. Young, 1983, On the simplification of generalized conjugate-gradient methods for nonsymmetrizable linear systems: Linear Algebra and its Applications, **52–53**, 399–417, doi: 10.1016/0024-3795(83)80026-3.

Kilmer, M. E., and E. de Sturler, 2006, Recycling subspace information for diffuse optical tomography: SIAM Journal on Scientific Computing, **27**, 2140–2166, doi: 10.1137/040610271.

Kim, S., and J. Pasciak, 2009, The computation of resonances in open systems using a perfectly matched layer: Mathematics of Computation, **78**, 1375–1398, doi: 10.1090/S0025-5718-09-02227-3.

Knizhnerman, L., V. Druskin, and M. Zaslavsky, 2009, On optimal convergence rate of the rational Krylov subspace reduction for electromagnetic problems in unbounded domains: SIAM Journal on Numerical Analysis, **47**, 953–971, doi: 10.1137/080715159.

Moskow, S., V. Druskin, T. Habashy, P. Lee, and S. Davydycheva, 1999, A finite difference scheme for elliptic equations with rough coefficients using a Cartesian grid nonconforming to interfaces: SIAM Journal on Numerical Analysis, **36**, 442–464, doi: 10.1137/S0036142997318541.

Remis, R., 1998, Reduced-order modeling of transient electromagnetic fields: Ph.D. thesis, Delft University of Technology.

Remis, R. F., 2004, Low-frequency model-order reduction of electromagnetic fields without matrix factorization: IEEE Transactions on Microwave Theory and Techniques, **52**, 2298–2304, doi: 10.1109/TMTT.2004.834577.

Remis, R. F., 2011, On the relation between FDTD and Fibonacci polynomials: Journal of Computational Physics, **230**, 1382–1386, doi: 10.1016/j.jcp.2010.11.009.

Remis, R. F., and P. M. van den Berg, 1998, Efficient computation of transient diffusive electromagnetic fields by a reduced modeling technique: Radio Science, **33**, 191–204, doi: 10.1029/97RS03693.

Ruhe, A., and D. Skoogh, 1998, Rational Krylov algorithms for eigenvalue computation and model reduction: International Workshop on Applied Parallel Computing. Large Scale Scientific and Industrial Problems, 491–502.

Sorensen, D. C., 2003, Passivity preserving model reduction via interpolation of spectral zeros: European Control Conference (ECC), 974–978.

Zimmerling, J., L. Wei, P. Urbach, and R. Remis, 2016, Efficient computation of the spontaneous decay rate of arbitrarily shaped 3D nanosized resonators: A Krylov model-order reduction approach: Applied Physics A, **122**, 158, doi: 10.1007/s00339-016-9643-4.